Clays and Clay Minerals, Vol. 59, No. 1, 13–20, 2011.

SIMULTANEOUS INTERCALATION OF TWO QUATERNARY PHOSPHONIUM SALTS INTO MONTMORILLONITE

SAHELI GANGULY, KAUSIK DANA, TAPAS KUMAR MUKHOPADHYAY, AND SANKAR GHATAK*

Advanced Clay and Traditional Ceramics Division, Central Glass and Ceramic Research Institute (CGCRI), CSIR, Kolkata-700032, India

Abstract—Intercalation of montmorillonites with a mixture of intercalates has not been studied extensively. The objective of the present investigation was to study the effects of phosphonium-based intercalate mixtures on the properties (organic loading and basal spacing) of montmorillonite. These phosphonium-intercalated montmorillonites are promising candidates as high-temperature stable nanofillers for application in clay polymer nanocomposites.

Two salts with different cationic heads and chain lengths were mixed in varying molar ratios and the mixtures were intercalated into the interlayer space of montmorillonite. Two sets were chosen based on the chain length and the cationic head-group structure of the two intercalated salts (referred to hereafter as set 1 and set 2). The resultant intercalated montmorillonite was characterized by thermogravimetric analysis, X-ray diffraction, and transmission electron microscopy. The organic loading of the intercalated montmorillonite increased with the proportion of longer carbon-chain intercalate in the mixture. The intensity of the characteristic XRD peak of each intercalate varied with the mole fraction percent of that intercalate in the solution mixture. No marked synergistic effect of the intercalate mixture on the basal spacing and organic loading properties of the intercalated montmorillonite was observed – the proportional influence of individual components was found to be more prominent.

Key Words—Basal Spacing, Intercalation, Mixed Intercalates, Montmorillonite, Organic Loading, Phosphonium Salts.

INTRODUCTION

Surface modifications of clay minerals are studied because they allow the creation of novel materials and, hence, materials with novel applications. During the past decade, organically modified layer silicates have received much attention from the scientific and technological communities because of their use as fillers in clay-polymer nanocomposites (CPN). The automotive, aerospace, and packaging industries view CPNs as promising materials for the 21st century due to their improved mechanical- and thermal-barrier and flame-retardant properties (Alexandre and Dubois, 2000; Zhu *et al*., 2001; Sinha Ray and Okamoto, 2003; Ruiz-Hitzky *et al*., 2004; Bergaya *et al*., 2006; Carrado and Bergaya, 2007; Hrachova *et al*., 2009). The surface energy, structural features, and chemical characteristics of the clay minerals and the viscosity of the polymer matrix are key factors in ensuring the desired properties of the nanocomposite. Modification of clay minerals with organic materials is necessary to establish compatibility between the clay particles and the polymer matrix. Apart from the CPN applications, these intercalated montmorillonites are also used as rheological modifiers, as adsorbents of pollutants in waste-water treatments, as thickening and gelling agents in paints and lubricants (Patel *et al*., 2006), and as drug-delivery vehicles for pharmaceutical purposes, *etc*. (Maguy and Lambert, 2010). Montmorillonite is the best of the smectite group of clay minerals for intercalation with organics because of its cation exchange capacity (CEC), swelling behavior, adsorption ability, and large surface area. The intercalation of organic cations into the interlayer space of montmorillonite is of paramount importance in the formation of a CPN because it changes two particular characteristics of the montmorillonite which help make it compatible with the hydrophobic polymer. Firstly, the intercalation changes the hydrophilic nature of the clay mineral to organophilic through ion exchange with the organic cations and, secondly, it increases the basal spacing which enhances the potential for delamination of clay platelets within the polymer matrix. The organic loading and basal spacing of the intercalated montmorillonite are, therefore, important properties because the degree of dispersion of the clay mineral in the polymer matrix depends on them. The dependence of the basal spacing and organic loading of intercalated montmorillonite with different organic intercalates is, therefore, worth studying. A considerable amount of work has been done using different intercalates with varying chain lengths and varying relative proportions (Xie *et al*., 2001, 2002; Fajnor and Hlavaty, 2002; Liu *et al*., 2007; Xi *et al*., 2007; Onal and Sarikaya, 2008; Avalos *et al*., 2009; Guegan *et al*., 2009; Li and Jhang, 2009). Novel oriented transparent films of layered silica-surfactant nanocomposite were synthesized by Ogawa in studies in which the chain length of the surfactants was

* E-mail address of corresponding author:
sghatak@cgcri.res.in
DOI: 10.1346/CCMN.2011.0590104

varied (Ogawa, 1994). Espina *et al*. (1998) discussed the effect of simultaneous intercalation in another layered system – they reported simultaneous intercalation of two n-alkyl amines into α-titanium phosphate systems and obtained new individual intercalation phases. Earlier studies which showed that basal spacing of intercalated montmorillonite depends on the orientation, organization, and population of the intercalate moieties dealt with a single intercalate only. In a more recent study, using a mixture of cationic and anionic intercalates, synergistic changes in basal spacings, organic loadings, adsorption, and adsorption capacity of the modified clay minerals (Chen *et al*., 2008) were reported. The influence of the structures of each intercalate within the mixture on the properties of the montmorillonites have yet to be explored. The limited thermal stability (<250ºC) of conventional organo-ammonium intercalated montmorillonite reduces the expected improvements in the CPN properties. The current challenge is to prepare a nanofiller that can withstand higher melt-processing temperatures (>300ºC), long residence times under high shear, and is stable in thermoset resins with high curing temperatures. Phosphonium-intercalated montmorillonites are promising candidates as high-temperature stable nanofillers for application in CPNs (Xie *et al*., 2002). For the present study, a synergistic composition was formulated by varying the cationic headgroup structure of two phosphonium-based intercalate mixtures to increase both the basal spacing and the organic loading of the montmorillonite.To the best of the authors' knowledge, no detailed study has been published on simultaneous intercalation using mixed phosphonium intercalates with varying cationic head groups and chain lengths. In the present investigation, two alkyl phosphonium intercalates with different chain lengths and cationic head-group structures (groups attached to the phosphorous of the phosphonium salt) were chosen. They were mixed with each other in different molar ratios and the resulting solution mixtures were intercalated simultaneously within the interlayer space of montmorillonite to observe its effect on basal spacing and organic loading.

EXPERIMENTAL

Materials

The <2 μm size fraction of (d_{50} = 0.85 μm, Mastersizer 2000, Malvern Instruments) montmorillonite (Mt) obtained from PGV (Nanocor, Arlington Heights, Illinois, USA) was used because of its large CEC value of 88 cmol kg^{-1}, which was primarily responsible for its effective susceptibility to intercalation. The CEC was measured using the EDTA-titrimetric method based on the alkali or alkaline-earth cation-exchange principle (Mehlich, 1948; Bache, 1976; Hillier and Clayton, 1992; Bergaya *et al*., 2006). The intercalates (bromide salts of hexadecyltributylphosphonium, Bu_3C_{16}; dodecyltriphenylphosphonium, Ph_3C_{12}; and tetrabutylphosphonium, Bu_4) were obtained from Sigma-Aldrich, St. Louis, Missouri, USA.

Method of simultaneous intercalation

In set 1, 0.01 M Bu_4 and Bu_3C_{16} salts were mixed with each other in different molar ratios for seven compositions (Table 1). A similar preparation method was followed for set 2 using Ph_3C_{12} and Bu_4 salts (Table 1). The intercalation procedure was as follows. 1 g of Na^+-exchanged montmorillonite (Na-Mt) was dispersed in 250 mL of deionized water by sonication (0.5 W cm^{-2}). 200 mL of mixed intercalate solution was added dropwise to this suspension with constant stirring. The entire intercalation was carried out at ~70–80ºC. The reaction mixture was allowed to settle overnight. The supernatant water with excess surfactant was decanted and the floc was redispersed. The process was repeated three times and then the floc was filtered under suction and washed with 2000 mL of hot double distilled water. The product collected was dried at 70ºC in vacuum for ~24 h. The dried product was ground in an agate mortar and kept in sealed glass bottles.

Characterization of intercalated montmorillonite

The thermal nature and organic loading were calculated from thermogravimetric analysis (TGA). The interlayer spacing was deduced from X-ray diffraction (XRD) analysis and verified by transmission electron microscopy (TEM).

TG analysis. The TG analysis of the samples was carried out using an OKAY instrument from Bysakh and Co., India. The system was operated at a heating rate of 10ºC min^{-1} from 30 to 800ºC in ambient atmosphere with ~50 mg of sample in an alumina crucible.

XRD analysis. The basal spacings of the montmorillonite and the intercalated montmorillonite were measured using an XPERT-PRO diffractometer (Panalytical). The system was operated at 30 mA and 40 kV between 2.0 and 10.0º2θ at a stepsize of 0.05º2θ.

TEM analysis. Transmission electron microscopy studies of the raw and intercalated clay mineral were performed using a Tecnai G^2 30 S-T transmission electron

Table 1. Compositions (mole fraction %) of set 1 and set 2.

Bu_4	Bu_3C_{16}	Set 1	Set 2	Bu_4	Ph_3C_{12}
0	100	MH100	MD100	0	100
20	80	MH80	MD80	20	80
40	60	MH60	MD60	40	60
50	50	MH50	MD50	50	50
60	40	MH40	MD40	60	40
80	20	MH20	MD20	80	20
100	0	MH0	MH0	100	0

https://doi.org/10.1346/CCMN.2011.0590104 Published online by Cambridge University Press

microscope (FEI Company, Hillsboro, Oregon, USA). The instrument filament was of LaB_6, the line resolution and point resolution were 1.4 Å and 2.0 Å, respectively, and the instrument was operated at 300 kV during the investigation.

Calculation of organic loading

The organic decomposition of intercalated montmorillonite started at >300ºC. The loss below that temperature was due to interlayer water, *i.e.* incomplete removal and/or moisture resorption after intercalation. The organic-loading calculation must consist of the mass loss corresponding to organics only; the loss of interlayer water of intercalated montmorillonites and the loss of structural water (dehydroxylation) of the raw montmorillonite must be excluded from the total mass loss of intercalated montmorillonite (mass loss corresponding to the heating region from 35 to 800ºC). The calculation uses the expression

$$c-(a+b) = \text{organic loading (mass\%)}$$

where,

a = Mass loss (mass%) corresponding to interlayer water up to 300ºC

b = Mass loss (mass%) corresponding to structural dehydroxylation from raw montmorillonite, *i.e.* mass loss from 500ºC to 800ºC

c = Total mass loss (mass%) of each intercalated montmorillonite

RESULTS AND DISCUSSION

Thermogravimetric analysis

The TG studies (in ambient atmosphere) of raw montmorillonite revealed two major temperature regions of mass loss. In the first step, adsorbed water was lost at temperatures up to 250–300ºC. The second step was dehydroxylation of montmorillonite which occurred between 500 and 800ºC. After intercalation, further mass loss occurred within the temperature region 300–500ºC due to the decomposition of incorporated organic molecules. Similar observations have been made by Xie *et al*. (2001, 2002). Different solution mixtures were made by varying the mole fraction percentages of component intercalates for intercalation in montmorillonite (Table 1). Each resultant intercalated montmorillonite, with different compositions of mixtures of set 1, was subjected to TG analysis in order to calculate the organic loading. The TG curves, one corresponding to each composition, showed the trend of mass loss with temperature (Figure 1). The organic loadings were calculated from mass-loss data available from TGA (Table 2); the values were related to the total amount of organics which were included within the montmorillonite, including any excess adsorbed as well as intercalated phosphonium salts. In intercalated montmorillonite, most of the intercalates were strongly anchored at the interlayer cation-exchange sites by electrostatic interaction. The remaining intercalates were anchored at the edges and faces of the clay particles, or by van der Waals' attraction with intercalated alkyl chains; these weakly linked intercalates were decomposed at much lower temperatures during heating than the more strongly attached intercalated molecules. The excess adsorption depends on the chain lengths of intercalates and the CEC of the montmorillonite (Ganguly *et al*., 2010). The organic-loading data reported here include both intercalated and excess adsorbed molecules. However, organic loading increased steadily with increase in mole fraction percent of Bu_3C_{16}, *i.e*. a longer chain (C16) component in the solution

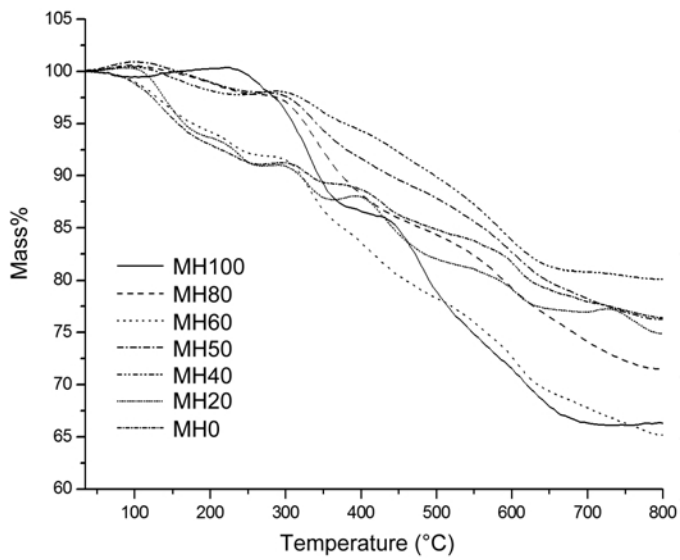

Figure 1. TG plots of intercalated montmorillonite set 1.

https://doi.org/10.1346/CCMN.2011.0590104 Published online by Cambridge University Press

Table 2. Calculation of organic loading of set 1-intercalated montmorillonite (Mt).

Set 1	Structural loss of raw Mt (mass%) (*b*)	Loss up to 300ºC (mass%) (*a*)	Total loss (mass%) (*c*)	Organic loading (mass%) {*c*−(*a*+*b*)}
MH100	4	4	34	26
MH80	4	3	29	22
MH60	4	9	35	22
MH50	4	3	24	17
MH40	4	2	20	14
MH20	4	10	26	12
MH0	4	9	24	11

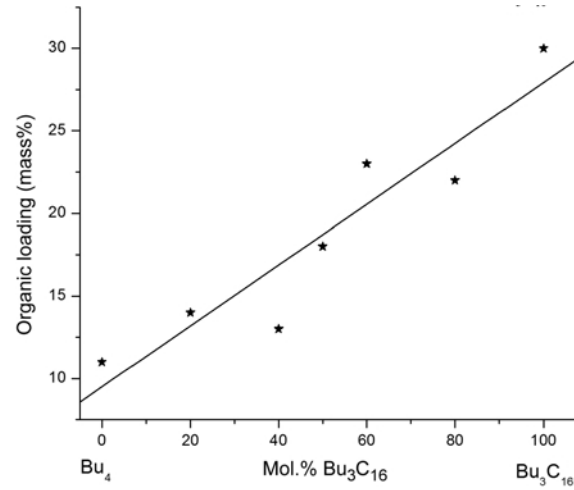

Figure 2. Plot of organic loading *vs*. mol.% of Bu_3C_{16}.

mixture. The TG plots (Figure 2) showed that the positive slope of the linear increment was 0.16. When 100% Bu_4 (denoted MH0 composition) had been intercalated, the organic loading was much less (~11 mass%) compared with that of 100% Bu_3C_{16} (denoted MH100 composition), where organic loading was 26 mass%. For all other compositions, the organic loading increased with the mole fraction percent of the longer-chain component (Bu_3C_{16}) of the mixture. The increase in organic loading with the longer-chain component can be explained by the increased van der Waals' attraction which led to the organic inclusion. A similar trend was observed in the TGA study of the set 2 compositions (Figure 3) in which Bu_4 (C4 with a tributyl head group) was common but Ph_3C_{12} (C12 with a triphenyl head group) was used as a second component to examine the effect of the cationic head group. The organic loading values for montmorillonite intercalated with set 2 intercalates were similarly related to the total organic content (as mentioned for set 1 [Table 3]). All of the organic loading values were between 30 and 11 mass%, *i.e.* the largest and smallest values of organic loading when 100% Ph_3C_{12} (MD100) and 100% Bu_4 (MH0) were intercalated, respectively. The linear increment of organic loading with increase in the longer-chain component was also observed here (Figure 4). The plot demonstrated that the slope of the linear increment was 0.21 compared to 0.16 for set 1. The difference in slope may be due to changes in the cationic head group and chain lengths in the set 2 intercalate compositions. These observations suggest that the organic loading during intercalation with mixed intercalates depended primarily on the contribution of the component with greater chain length.

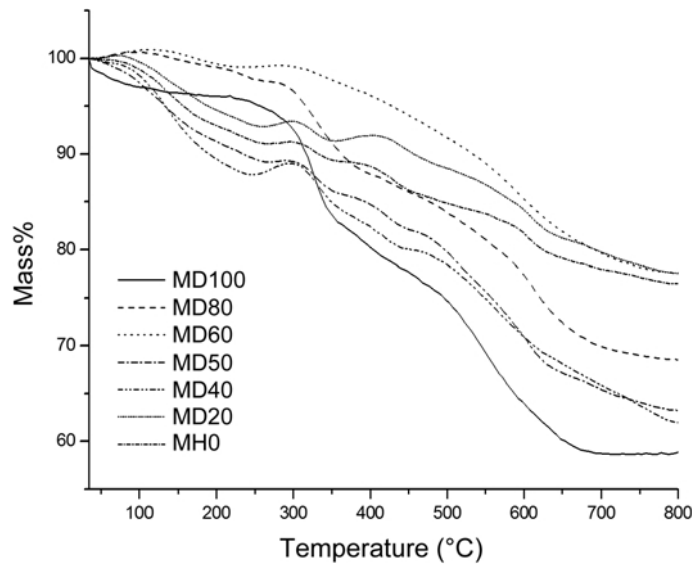

Figure 3. TG plots of intercalated montmorillonite set 2.

https://doi.org/10.1346/CCMN.2011.0590104 Published online by Cambridge University Press

Table 3. Calculation of organic loading of set 2-intercalated montmorillonite (Mt).

Set 2	Structural loss of raw Mt (mass%) (*b*)	Loss up to 300ºC (mass%) (*a*)	Total loss (mass%) (*c*)	Organic loading (mass%) {*c*−(*a*+*b*)}
MD100	4	7	41	30
MD80	4	4	32	24
MD60	4	1	23	18
MD50	4	11	37	22
MD40	4	12	38	22
MD20	4	7	23	12
MD0	4	9	24	11

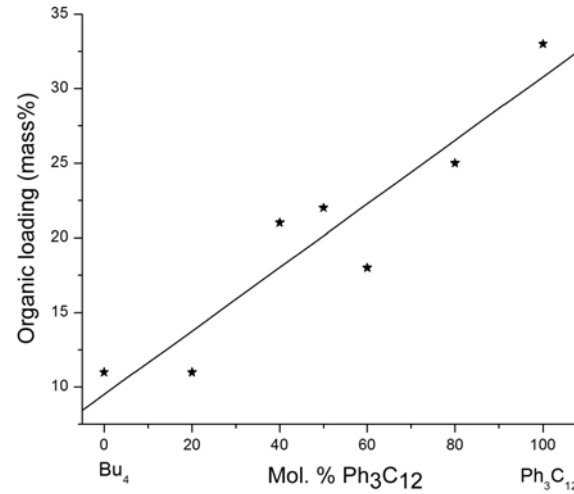

Figure 4. Plot of organic loading *vs*. mol.% of Ph_3C_{12}.

X-ray diffraction analysis

The arrangement of the interlayer of intercalated montmorillonite was elucidated by XRD analysis. Na-montmorillonite has a basal spacing (d_{001}) of ~1.25 nm (Theng, 1974; Bergaya *et al*., 2006). The smectite group of minerals shows variable integral series of basal spacings (d_{00l}), which depends on the size of the exchangeable cation and on the degree of hydration of the cation (Grim, 1968). The XRD traces of intercalated montmorillonite (Figure 5) revealed that intercalation by ion exchange with the phosphonium intercalates mixture increased the basal spacing of raw montmorillonite due to replacement of smaller interlayer Na^+ by the larger phosphonium ions. When montmorillonite was intercalated with 100% Bu_4 (MH0), two peaks appeared, one at 2.10 nm and one at 1.66 nm (Figure 5). The peaks were moderately sharp and well defined. A similar, single sharp peak, corresponding to a basal spacing of 2.71 nm with a small hump, appeared for 100% Bu_3C_{16} (MH100) intercalated montmorillonite. When montmorillonite was intercalated with mixtures of different compositions, the XRD peaks broadened, diffused, and were rather difficult to identify. Most of the peaks were shifted from the characteristic one obtained from the MH100 and MH0 compositions. To deal with the problem, the XRD plots were broadly divided into two regions based on the characteristic XRD peak patterns. One was the Bu_3C_{16}

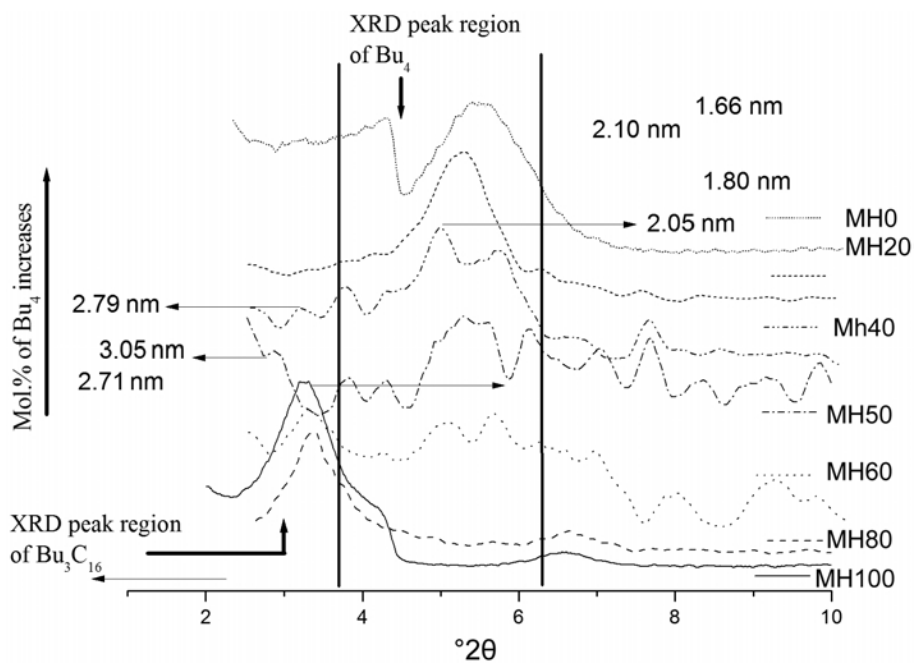

Figure 5. XRD plots of hybrid set 1.

https://doi.org/10.1346/CCMN.2011.0590104 Published online by Cambridge University Press

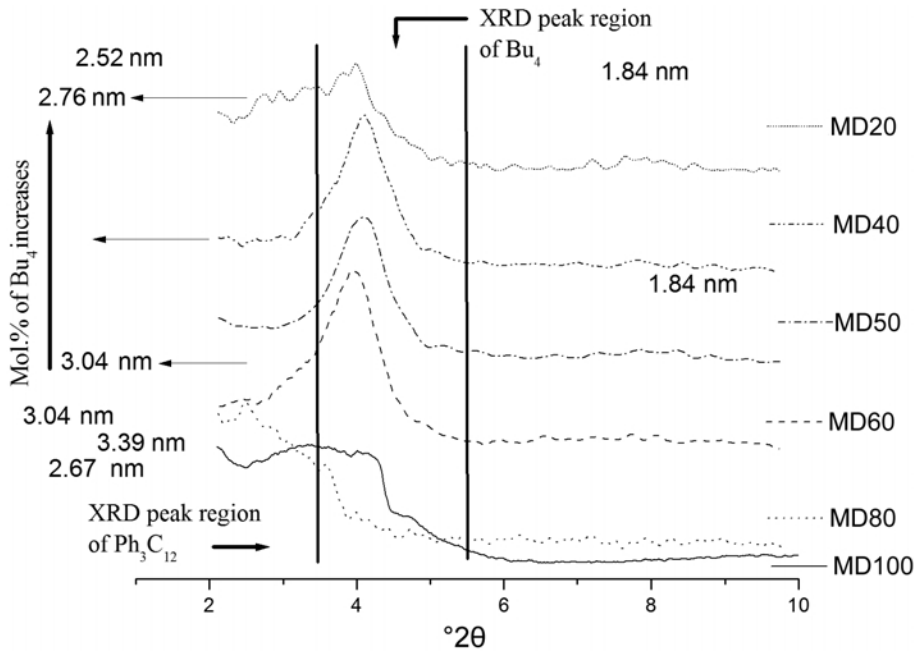

Figure 6. XRD plots of hybrid set 2.

peak region and the other was the Bu_4 peak region. The division is marked clearly in Figure 5. The XRD patterns for intercalated montmorillonites with different compositions in sets 1 and 2 (Figures 5 and 6 and summarized in Tables 4 and 5, respectively) clearly demonstrated that the multiple XRD peaks were due to heterogeneous mixed-layer arrangements of intercalated organics within the interlayer space of montmorillonite. In the set 1 composition (Table 4), the d_{001} values in the Bu_3C_{16} peak region closely matched paraffinic layer orientation of the intercalated organics whereas the d_{001} values of the Bu_4 region showed a mixed paraffinic and bilayer arrangement of intercalates (Theng, 1974; Li and Ishida, 2002; Ganguly *et al*., 2010). The coexistence of different interlayer arrangements of intercalates in montmorillonite was the source of the interlayer heterogeneity. Superimposition of reflections corresponding to these different interlayer distances created the multiple, wide, and diffuse peaks (Zidelkheir and Abdelgoad, 2008). In set 2 compositions (Table 5), the d_{001} values of the Ph_3C_{12} and Bu_4 peak regions resembled paraffinic and bilayer arrangements, respectively. Multiple peaks in MD40 and MD20 demonstrated that layer heterogeneity was also present, but to a lesser extent than for set 1 compositions. Closer inspection of resultant XRD patterns of intercalated montmorillonite with set 1 compositions (Figure 5) revealed that, with variation in the mole fraction percent of each component, the intensity of the characteristic XRD peak of that component varied. The patterns also revealed that, as the mole fraction percent of Bu_4 increased in the solution mixture, the intensity of the characteristic peaks of Bu_4 (2.10 nm and 1.66 nm) increased with the gradual disappearance of the 2.71 nm peak for Bu_3C_{16}. Peaks were shifted and overlapped because of mixing of intercalates; however, the characteristic peak pattern of each component within its peak

Table 4. d_{001} values and interlayer arrangements of organo-montmorillonite intercalated with set 1 compositions.

Set 1	—— Bu_3C_{16} peak region ——		—— Bu_4 peak region ——	
	d_{001} (nm)	Interlayer arrangement	d_{001} (nm)	Interlayer arrangement
MH100	2.71	Paraffinic	–	–
MH80	2.72	Paraffinic	–	–
MH60	2.69	Paraffinic	1.75,1.55	Bilayer
MH50	3.05	Paraffinic	2.05,1.67	Paraffinic, Bilayer
MH40	2.79	Paraffinic	2.05,1.80	Paraffinic, Bilayer
MH20	–	–	2.20,1.68	Paraffinic, Bilayer
MH0	–	–	2.10,1.66	Paraffinic, Bilayer

https://doi.org/10.1346/CCMN.2011.0590104 Published online by Cambridge University Press

Table 5. d_{001} values and interlayer arrangements of organo-montmorillonite intercalated with set 2 compositions.

Set 2	—— Ph_3C_{12} peak region ——		—— Bu_4 peak region ——	
	D_{001} (nm)	Interlayer arrangement	d_{001} (nm)	Interlayer arrangement
MD100	3.39, 2.67	Paraffinic	–	–
MD80	3.04	Paraffinic	–	–
MD60	3.04	Paraffinic	1.84	Bilayer
MD50	–	–	1.80	Bilayer
MD40	2.85,2.52	Paraffinic	1.76	Bilayer
MD20	2.76,2.52	Paraffinic	1.84	Bilayer
MH0	–	–	2.10,1.66	Paraffinic, Bilayer

region could be identified from the XRD plots. At 80% mole fraction of Bu_4 in the mixture (MH20), a prominent peak at 1.68 nm with a small hump at 2.20 nm appeared and the characteristic peak for Bu_3C_{16} was absent. Though the most widely used technique to determine the structure and arrangement of the organic cations in the interlayer space of montmorillonite is XRD, it gives only average structural information. The local microstructures and morphology of intercalated montmorillonite can be best viewed by means of TEM. A representative TEM image of composition MH20 (Figure 7) shows a well defined layer stacking separated by regular van der Waals' gaps or interlayer spaces. Variation of arrangements can be observed by both fringe contrast and fringe spacing. Equal contrasts suggest arrangement of the same orientation along the *c* axis (Marcovich *et al*., 2005). The *d* spacing of MH20 (20 mol.% of Bu_3C_{16}), obtained from the TEM image, was 1.7 nm. A closer inspection of the XRD plot of MH20 (Figure 5) revealed a prominent XRD peak at 1.68 nm, one of the characteristic peaks of Bu_4. The characteristic peak of Bu_3C_{16} had almost disappeared. The 1.7 nm basal spacing obtained from the TEM study was reasonable and supported the XRD results. The XRD analysis of the intercalated montmorillonite of set 2 followed a similar trend as in set 1. The plots (Figure 6) showed that 100% Ph_3C_{12} (MD100) intercalated montmorillonite yielded an XRD peak at 2.67 nm with a small hump at 3.39 nm, and 100% Bu_4 (MH0) gave peaks at 2.10 nm and 1.66 nm as mentioned previously. A similar variation in the intensity of the characteristic peaks of each component with their mole fraction percent was also observed. Another important feature from the XRD plot (Figure 6) was that, for 80% Bu_4 (MD20) intercalated montmorillonite, a relatively sharp peak appeared at 1.84 nm in the Bu_4 peak region. This characteristic peak of Bu_4 (MH0) shifted marginally from 1.66 nm. The nature of the XRD patterns also indicated that the components were not combining to give a single basal spacing. The appearance and disappearance of individual characteristic peaks corresponding to each component and its mole fraction percent in the mixture again confirmed the absence of any synergistic effect. The intensity of the XRD peaks of a component depended on the proportion of that component in the solution mixture only. As shown by TGA and subsequently confirmed by XRD analysis, the mixing of two cationic intercalates during simultaneous intercalation in montmorillonite manifested a proportionate contribution of the individual intercalates.

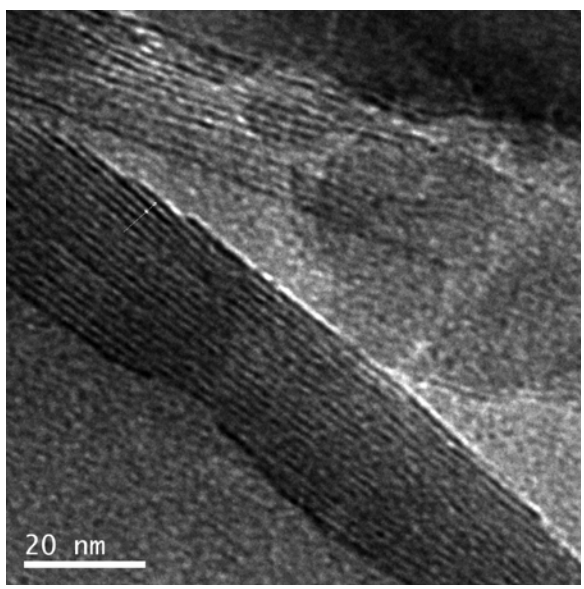

Figure 7. TEM image of sample MH20.

CONCLUSIONS

(1) During simultaneous intercalation of montmorillonite layers with mixtures of two intercalates, organic loading of the montmorillonite increased linearly with increase in the mole fraction percent of the longer-chain component of the intercalate mixture.

(2) The characteristic XRD peak intensity and interlayer spacing for each individual intercalate varied with its mole fraction percent in the mixture. As the mole fraction percent of a particular component of the mixture increased, the intensity of the characteristic XRD peak of that component increased with the gradual disappearance of the XRD peak of the other component.

https://doi.org/10.1346/CCMN.2011.0590104 Published online by Cambridge University Press

(3) Simultaneous intercalation with mixtures of two intercalates in montmorillonite manifested the effect of each individual component in the mixture.

ACKNOWLEDGMENTS

The work was supported by a CSIR fellowship grant to Saheli Ganguly (currently working as a senior research fellow in CGCRI, Kolkata, India). The authors thank the XRD, Instrumentation and TEM section of CGCRI for providing access to the analytical facilities.

REFERENCES

Alexandre, M. and Dubois, P. (2000) Polymer-layered silicate nanocomposites: preparation, properties and uses of a new class of materials. *Materials Science and Engineering Report*, **28**, 1–63.

Avalos, F., Ortiz, J.C., Zitzumbo, R., Manchado, M.A.L., Verdejo, R., and Arroyo, M. (2009) Phosphonium salt intercalated montmorillonites. *Applied Clay Science*, **43**, 27–32.

Bache, B.W. (1976) The measurement of cation exchange capacity of soils. *Journal of the Science of Food and Agriculture*, **27**, 273–280.

Bergaya, F., Lagaly, G., and Vayer, M. (2006) Cation and anion exchange. Pp. 979–1001 in: *Handbook of Clay Science* (F. Bergaya, B.K.G. Theng, and G. Lagaly, editors). Developments in Clay Science, Vol. **1**, Elsevier Ltd., Amsterdam.

Bergaya, F., Theng, B.K.G., and Lagaly, G. (2006) *Handbook of Clay Science*. Developments in Clay Science, Vol. **1**, Elsevier Ltd., Amsterdam.

Carrado, K.A. and Sandi, G., (2007) Metal nanoclusters on polymer-clay nanocomposite films. Pp. 298 in: *Polymer-Clay Nanocomposite Research* (K.A. Carrado and F. Bergaya, editors). CMS workshop lectures, Vol. **15**, The Clay Minerals Society, Aurora, Colorado.

Chen, D., Zhu, J.X., Yuan, P., Yang, S.J., Chen, T.-H., and He, H.P. (2008) Preparation and characterization of anion-cation surfactants modified montmorillonite. *Journal of Thermal Analysis and Calorimetry*, **94**, 841–848.

Emmerich, K., Wolters, F., Kahr, G., and Lagaly, G. (2009) Clay profiling: The classification of montmorillonites. *Clays and Clay Minerals*, **57**, 104–114.

Espina, A., Jaimez, E., Khainakov, S.A., Trobajo, C., Garcia, J.R., and Rodriguage, J. (1998) Synthesis of n-alkylamines intercalation compounds with α-titanium phosphate. Process selectivity and structural and morphological characterization. *Chemistry of Materials*, **10**, 2490–2496.

Fajnor, V.S. and Hlavaty, V. (2002) Thermal stability of clay/organic intercalation complexes. *Journal of Thermal Analysis and Calorimetry*, **67**, 113–118.

Ganguly, S., Dana, K., and Ghatak, S. (2010) Thermogravimetric study of *n*-alkylammonium-intercalated montmorillonites of different cation exchange capacity. *Journal of Thermal Analysis and Calorimetry*, **100**, 71–78.

Grim, R.E. (1968) *Clay Mineralogy*. 2nd edition, McGraw-Hill, Columbus, Ohio, USA.

Guegan, R., Gautier, M., Beny, J.M., and Muller, F. (2009) Adsorption of a C10E3 non-ionic surfactant on a Ca-smectite. *Clays and Clay Minerals*, **57**, 502–509.

Hillier, S. and Clayton, T. (1992) Cation exchange 'staining' of clay minerals in thin-section for electron microscopy. *Clay Minerals*, **27**, 379–384.

Hrachova, J., Komadel, P., and Chodak, I. (2009) Natural rubber nanocomposites with organo-modified bentonites. *Clays and Clay Minerals*, **57**, 444–451.

Li, Y. and Ishida, H. (2002) A differential scanning calorimetry study of the assembly of hexadecylamine molecules in the nanoscale confined space of silicate galleries. *Chemistry of Materials*, **14**, 1398–1404.

Li, Z. and Jhang, W.T. (2009) Interlayer conformations of intercalated dodecyltrimethylammonium in rectorite as determined by FTIR, XRD, and TG analysis. *Clays and Clay Minerals*, **57**, 194–204.

Liu, X., Lu, X., Wang, R., Zhou, H., and Xu, S. (2007) Interlayer structure and dynamics of alkyl-ammonium-intercalated smectites with and without water: a molecular dynamics study. *Clays and Clay Minerals*, **55**, 554–564.

Maguy, J. and Lambert, J.F. (2010) A new nanocomposite: LDOPA/Laponite. *Journal of Physical Chemistry Letters*, **1**, 85–88.

Marcovich, D.Y., Chen,Y., Nir, S., and Prost, R. (2005) High resolution electron microscopy structural studies of organo-clay nanocomposites. *Environmental Science and Technology*, **39**, 1231–1238.

Mehlich, A. (1948) Determination of cation- and anion-exchange properties of soils. *Soil Science*, **66**, 429–445.

Ogawa, M. (1994) Formation of novel oriented transparent films of layered silica-surfactant nanocomposites. *Journal of the American Chemical Society*, **116**, 7941–7942.

Onal, M. and Sarikaya, Y. (2008) Thermal analysis of some organo clays. *Journal of Thermal Analysis and Calorimetry*, **91**, 261–265.

Patel, H.A., Somani, R.S., Bajaj, H.C., and Jasra, R.V. (2006) Nanoclays for polymer nanocomposites, paints, inks, greases and cosmetics formulations, drug delivery vehicle and waste water treatment. *Bulletin of Materials Science*, **29**, 2, 133–145.

Ruiz-Hitzky, E., Aranda, P., and Serratosa, J.M. (2004) Clay–organic interactions: organoclay complexes and polymer-clay nanocomposites. Pp. 91–154 in: *Handbook of Layered Materials* (S. Auerbach, K.A. Carrado, and P. Dutta, editors). Marcel Dekker, New York.

Sinha Ray, S. and Okamoto, M. (2003) Polymer/layered nanocomposites: a review from preparation to processing. *Progress in Polymer Science*, **28**, 1539–1641.

Theng, B.K.G. (1974) *The Chemistry of Clay-Organic Reactions*. Wiley Interscience, New York.

Xi, Y., Zhou, Q., Frost, R., and He, H. (2007) Thermal stability of octadecyltrimethylammonium bromide-modified montmorillonite organo clay. *Journal of Colloid and Interface Science*, **311**, 347–353.

Xie, W., Gao, Z., Pan, W.P., Hunter, D., Singh, A., and Vaia, R. (2001) Thermal degradation chemistry of alkyl quaternary ammonium montmorillonite. *Chemistry of Materials*, **13**, 2979–2990.

Xie, W., Xie, R., Pan, W.P., Hunter, D., Koene, B., Tan, L.S., and Vaia, R. (2002) Thermal stability of quaternary phosphonium modified montmorillonites. *Chemistry of Materials*, **14**, 4837–4845.

Zhu, J., Morgan, A.B., Lamelas, F.J., and Wilkie, C.A. (2001) Fire properties of polystyrene–clay nanocomposites. *Chemistry of Materials*, **13**, 3774–80.

Zidelkheir, B. and Abdelgoad, M. (2008) Effect of surfactant agent upon the structure of montmorillonite. X-ray diffraction and thermal analysis. *Journal of Thermal Analysis and Calorimetry*, **94**, 181–187.

(*Received 28 April 2010; revised 20 January 2011; Ms. 431; A.E. F. Bergaya*)